

SCIENTIFIC REPORTS

OPEN

Improvement of thermoelectric properties and their correlations with electron effective mass in $\text{Cu}_{1.98}\text{S}_x\text{Se}_{1-x}$

Received: 10 October 2016
Accepted: 06 December 2016
Published: 16 January 2017

Lanling Zhao^{1,2}, Frank Yun Fei², Jun Wang³, Funing Wang¹, Chunlei Wang¹, Jichao Li¹, Jiyang Wang⁴, Zhenxiang Cheng², Shixue Dou² & Xiaolin Wang²

Sulphur doping effects on the crystal structures, thermoelectric properties, density-of-states, and effective mass in $\text{Cu}_{1.98}\text{S}_x\text{Se}_{1-x}$ were studied based on the electrical and thermal transport property measurements, and first-principles calculations. The X-ray diffraction patterns and Rietveld refinements indicate that room temperature $\text{Cu}_{1.98}\text{S}_x\text{Se}_{1-x}$ ($x = 0, 0.02, 0.08, 0.16$) and $\text{Cu}_{1.98}\text{S}_x\text{Se}_{1-x}$ ($x = 0.8, 0.9, 1.0$) have the same crystal structure as monoclinic- Cu_2Se and orthorhombic- Cu_2S , respectively. Sulphur doping can greatly enhance zT values when x is in the range of $0.8 \leq x \leq 1.0$. Furthermore, all doped samples show stable thermoelectric compatibility factors over a broad temperature range from 700 to 1000 K, which could greatly benefit their practical applications. First-principles calculations indicate that both the electron density-of-states and the effective mass for all the compounds exhibit non-monotonic sulphur doping dependence. It is concluded that the overall thermoelectric performance of the $\text{Cu}_{1.98}\text{S}_x\text{Se}_{1-x}$ system is mainly correlated with the electron effective mass and the density-of-states.

The dimensionless thermoelectric figure-of-merit (zT) is defined as $zT = S^2\sigma T/\kappa = S^2\sigma T/(\kappa_c + \kappa_l)$, where S , T , σ , κ , κ_c , and κ_l are the Seebeck coefficient, absolute temperature in Kelvin, electrical conductivity, total thermal conductivity, charge carrier thermal conductivity, and lattice thermal conductivity, respectively^{1–4}. Enhanced zT values could be realized through adjusting the electronic structures and thermal conductivity by the doping approach^{5–9}. It should be noted that zT is proportional to the square of S , indicating that improving S might be an easier way to get improved zT values, compared to regulating the other thermoelectric parameters such as σ and κ .

It is well known that σ and S can be estimated by the following formulas^{10–12},

$$\sigma = ne\mu \quad (1)$$

$$S = \frac{8\pi^2 k_B^2}{3eh^2} m^* T \left(\frac{\pi}{3n} \right)^{2/3} \quad (2)$$

where n , μ , k_B , h , and m^* are the charge carrier density, carrier mobility, Boltzmann constant, Planck constant and effective mass of the carriers, respectively. Moreover, the effective mass (m^*) and carrier mobility (μ) can be deduced from the electronic band structures and density-of-states (DOS) obtained from related first-principle calculations¹³. In this regard, S can be predicted through performing theoretical calculations on the electronic band structures and DOS, and the estimation of σ can also be roughly achieved with considering the average scattering time as a constant^{14,15}. Therefore, it is highly desirable to gain insight into the electronic structures to get theoretical backup for the observed experimental phenomena.

¹School of Physics, Shandong University, Jinan, 250100, P.R. China. ²Spintronic and Electronic Materials Group, Institute for Superconducting and Electronic Materials, Australian Institute for Innovative Materials, University of Wollongong, North Wollongong, 2500, Australia. ³Key Laboratory for Liquid-Solid Structural Evolution and Processing of Materials, Shandong University, Jinan, 250061, China. ⁴Institute for Crystal Materials, Shandong University, Jinan, 250100, P. R. China. Correspondence and requests for materials should be addressed to X.W. (email: xiaolin@uow.edu.au)

Among all the state-of-the-art high temperature *p*-type thermoelectric materials, the copper-ion-liquid-like Cu_{2-x}Se and Cu_{2-x}S compounds show high thermoelectric performance, even though there still are some issues that need to be resolved before practical applications can be considered¹⁶. It has been reported that polycrystalline Cu_{2-x}Se and Cu_{2-x}S bulks can achieve the highest zT values of around 1.6 and 1.7 at 1000 K^{17,18}, which have been further improved to 1.8 and 1.9^{19,20}, respectively.

Additionally, it should be noted that the high-temperature $\beta\text{-Cu}_{2-x}\text{Se}$ and $\alpha\text{-Cu}_{2-x}\text{S}$ have the same crystal structure, and both of them are superionic conductors. Besides the high crystal symmetry, these two systems also possess another important property, that of congruent melting, which means that highly dense samples can be easily fabricated by a facile melt-solidification technique.

The previous studies^{20–22} on the electronic structures for Cu_2Se and Cu_2S compounds indicate that the copper deficiency makes both of them intrinsic *p*-type conductors owing to the contributions mainly from the Cu 3d-, Se 4p-, and S 3p-states near the Fermi level (E_F). These facts provide evidence that doping other elements into Cu or Se (S) sites could effectively alter their electronic structures, and consequently affect their electrical and thermal transport behaviour as well as their overall thermoelectric performance.

Generally, in order to obtain enhanced S and concurrent high σ as well as low κ values through the doping approach, the following factors should be considered when choosing dopants: (1) Dopants should have the same valence as the counterpart element, which will ensure the charge balance of the system and maintain the same crystal structure. (2) Dopants should have comparable radiuses to the counterpart element, which will result in little difference in the lattice parameters and provide good optimization of electrical and thermal transport properties.

As for the Cu_{2-x}Se system, the doping approach, using such elements as Ag, Sb, Al, and Sn for the Cu sites^{23–28} and Te and I for the Se sites^{21,29}, has been chosen to modify its electronic structures and thermal conductivity up to now. The results illustrate, however, that only a small amount doping with one of these elements could lead to limited improvements to the thermoelectric performance in this system. Generally, the lighter atoms and heavier atoms should have opposite effects on the electronic and thermal transport properties. For the substitutions on Se sites, only the heavier atoms have been investigated so far, and no enhanced thermoelectric performance was observed except at the phase transition temperatures. Therefore, it is necessary to investigate the doping effects of lighter atoms, with a smaller atomic radius, to test whether or not the doping approach could be beneficial for the further enhancement of the overall thermoelectric performance of the Cu_{2-x}Se system.

In this work, we investigated sulphur doping effects on the thermoelectric properties of the Cu_{2-x}Se system based on the following considerations: (1) At high temperature, $\alpha\text{-Cu}_2\text{S}$ has the same crystal structure as $\beta\text{-Cu}_2\text{Se}$, and therefore, sulphur should be very easy to substitute into the lattice and replace Se. (2) S^{2-} has the same valence as Se^{2-} , which should result in good electron balance in this system. (3) The unit cell size should be reduced after S substitutes for Se, which will affect the migration of copper ions and lead to varied electrical and thermal transport behaviour.

It should be noted that, for practical applications of thermoelectric materials, besides the high zT values, the thermoelectric compatibility factor (s), derived as $s = \frac{\sqrt{1+zT}-1}{S \cdot T}$, is another important factor, which is crucial for the efficient operation of a high temperature thermoelectric device^{12,30–33}. The closer the s for two *n*- and *p*-type thermoelectric materials, the higher the combined efficiency that will be achieved when they are adjoining segments in one thermoelectric device. Little information on s , however, has been reported for the Cu_{2-x}Se or Cu_{2-x}S based thermoelectric materials. Hence, it is meaningful to calculate the s values for the sulphur doped Cu_{2-x}Se to gain sufficient information for their future practical applications.

Herein, the doping effects on the thermoelectric properties of highly dense $\text{Cu}_{1.98}\text{S}_x\text{Se}_{1-x}$ polycrystalline bulks were investigated experimentally, in order to provide a full understanding of how the doping approach modifies the thermoelectric properties of the Cu_{2-x}Se system. We also conducted a systematic study on the sulphur doping effects on the electronic band structures and DOS for the $\text{Cu}_{15}\text{S}_x\text{Se}_{8-x}$ compounds based on Density Functional Theory (DFT) calculations. The results indicate that the overall thermoelectric performance in $\text{Cu}_{1.98}\text{S}_x\text{Se}_{1-x}$ is strongly dependent on the sulphur doping concentration, and it is mainly correlated with the electron effective mass and DOS.

Results and Discussion

Figure 1 shows the X-ray diffraction (XRD) patterns for the fabricated $\text{Cu}_{1.98}\text{S}_x\text{Se}_{1-x}$ ($x = 0, 0.02, 0.08, 0.16, 0.2, 0.3, 0.4, 0.5, 0.6, 0.7, 0.8, 0.9, 1.0$) samples. The results indicate that the $\text{Cu}_{1.98}\text{S}_x\text{Se}_{1-x}$ samples show different crystal structures with different x values. They are single-phase and have the same monoclinic³⁴ crystal structure as the low temperature α -phase Cu_{2-x}Se (PDF No.: 27–1131²³) when $x \leq 0.16$. They then become composites of low temperature cubic structured $\text{Cu}_{1.8}\text{Se}$ and hexagonal structured $\text{Cu}_{2.001}\text{S}$ when x varies in the range from 0.2 to 0.7 ($0.2 \leq x \leq 0.7$). Finally, they become single-phase orthorhombic structured Cu_2S (PDF: 23–961) when x is over 0.8.

Rietveld refinements were performed for all samples based on the obtained X-ray diffraction patterns and the deduced lattice parameters, and the R-factors are listed in Table S1 (Supplementary Information). The summarized phase diagram for the sulphur doping level dependence of the lattice parameters is also displayed in Fig. 2, revealing that the $\text{Cu}_{1.98}\text{S}_x\text{Se}_{1-x}$ ($x = 0.02, 0.08, 0.16$) samples have slightly reduced lattice parameters in comparison with the $\text{Cu}_{1.98}\text{Se}$ sample, due to the smaller radius of sulphur compared to that of selenium. In the same way, the $\text{Cu}_{1.98}\text{S}_{0.8}\text{Se}_{0.2}$ and $\text{Cu}_{1.98}\text{S}_{0.9}\text{Se}_{0.1}$ samples have enlarged lattice parameters in contrast to the $\text{Cu}_{1.98}\text{S}$ sample, owing to the larger radius of selenium.

The geometry optimized primitive cells for the $\text{Cu}_{15}\text{S}_x\text{Se}_{8-x}$ ($x = 0, 1, 2, 4, 6, 8$) compounds are displayed in Figure S2, and the lattice parameters for these compounds are summarized in Table S1 which exhibit the consistent variation trend as the obtained experimental results. The $\text{Cu}_{15}\text{Se}_8$ has the largest volume of 387.606 \AA^3 , while

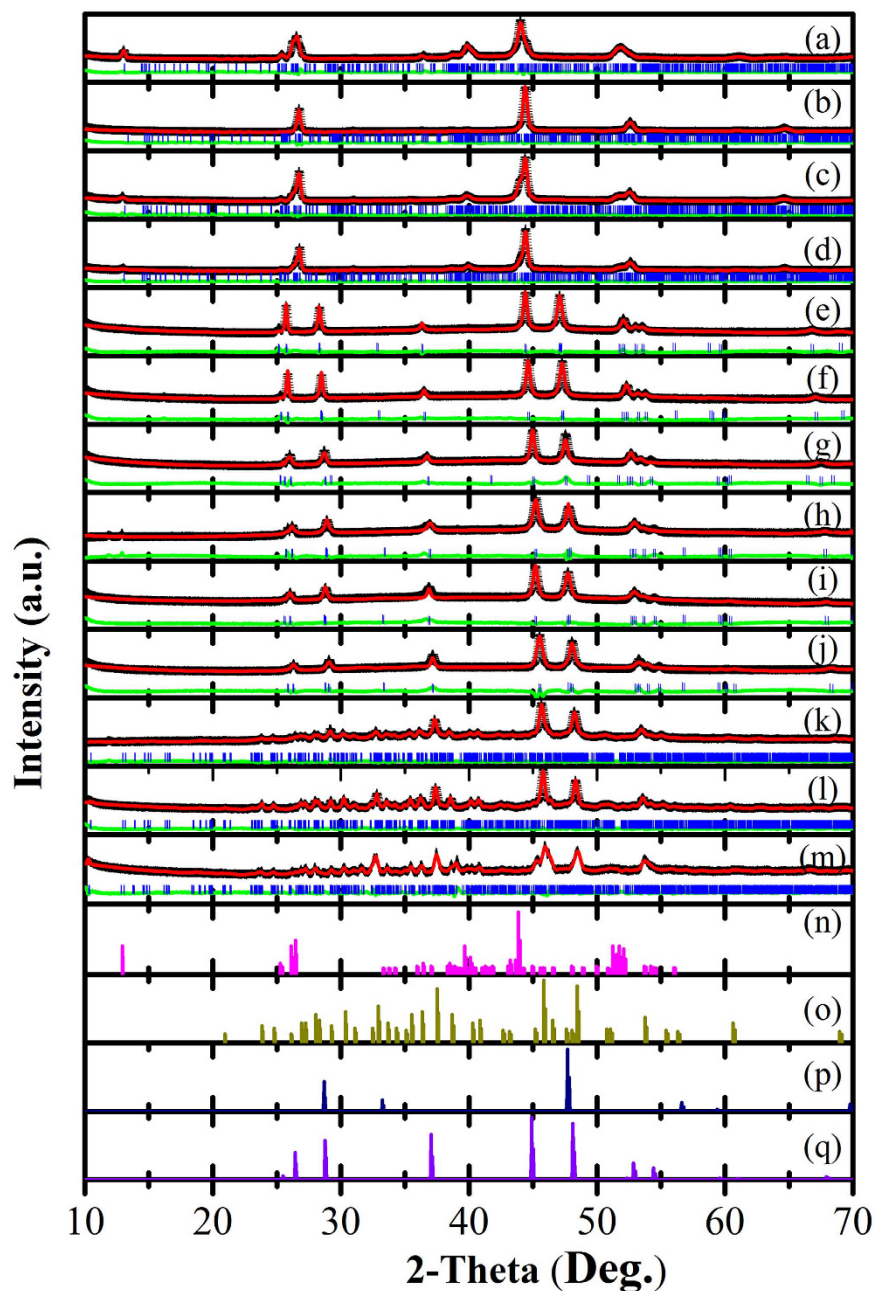


Figure 1. X-ray diffraction (XRD) patterns of the fabricated $\text{Cu}_{1.98}\text{S}_x\text{Se}_{1-x}$ ($x = 0, 0.02, 0.08, 0.16, 0.2, 0.3, 0.4, 0.5, 0.6, 0.7, 0.8, 0.9, 1.0$) samples: (a) $\text{Cu}_{1.98}\text{Se}$, (b) $\text{Cu}_{1.98}\text{S}_{0.02}\text{Se}_{0.98}$, (c) $\text{Cu}_{1.98}\text{S}_{0.08}\text{Se}_{0.92}$, (d) $\text{Cu}_{1.98}\text{S}_{0.16}\text{Se}_{0.84}$, (e) $\text{Cu}_{1.98}\text{S}_{0.2}\text{Se}_{0.8}$, (f) $\text{Cu}_{1.98}\text{S}_{0.3}\text{Se}_{0.7}$, (g) $\text{Cu}_{1.98}\text{S}_{0.4}\text{Se}_{0.6}$, (h) $\text{Cu}_{1.98}\text{S}_{0.5}\text{Se}_{0.5}$, (i) $\text{Cu}_{1.98}\text{S}_{0.6}\text{Se}_{0.4}$, (j) $\text{Cu}_{1.98}\text{S}_{0.7}\text{Se}_{0.3}$, (k) $\text{Cu}_{1.98}\text{S}_{0.8}\text{Se}_{0.2}$, (l) $\text{Cu}_{1.98}\text{S}_{0.9}\text{Se}_{0.1}$, (m) $\text{Cu}_{1.98}\text{S}$, (n) standard XRD pattern for monoclinic structured Cu_2Se , (o) standard XRD pattern for orthorhombic structured Cu_2S , (p) standard XRD pattern for cubic structured $\text{Cu}_{1.8}\text{Se}$, and (q) standard XRD pattern for hexagonal structured $\text{Cu}_{2.001}\text{S}$. (+ data points, – calculation line, – difference line, | marker points).

the Cu_{15}S_8 has the smallest volume of 340.486 \AA^3 . The $\text{Cu}_{15}\text{S}_x\text{Se}_{8-x}$ ($x = 1, 2, 4, 6$) compounds have the volume values between 352.784 and 378.266 with values decreased with increasing x .

Since both Cu_{2-x}Se and Cu_{2-x}S are superionic conductors, and the migration of copper ions plays important roles on the system's electrical conductivity, the changed lattice parameters should lead to different electrical conductivity and Seebeck coefficient, which will, in turn, result in modified thermoelectric properties with different zT values. Thus, it is essential to discuss the sulphur doping effects on the thermoelectric properties of the Cu_{2-x}Se system, as well as the selenium doping effects on the thermoelectric properties of the Cu_{2-x}S system. Hence, we will focus on the thermoelectric properties of the single-phase $\text{Cu}_{1.98}\text{S}_x\text{Se}_{1-x}$ ($x = 0.02, 0.08, 0.16$) and $\text{Cu}_{1.98}\text{S}_x\text{Se}_{1-x}$ ($x = 0.8, 0.9, 1.0$) samples in the following part.

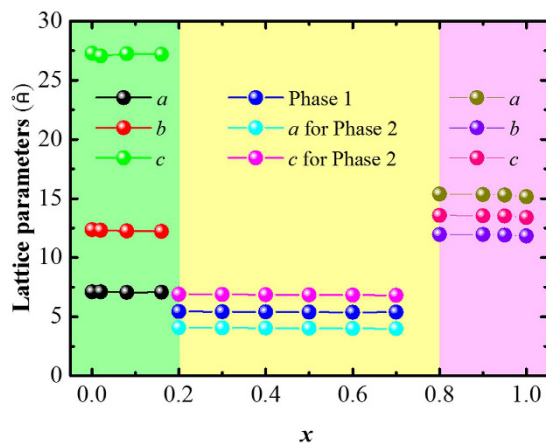


Figure 2. Phase diagram of sulphur doping level dependence of the crystal structures at room temperature. (I: monoclinic structured Cu_2Se phase; II: Composites of cubic structured $\text{Cu}_{1.8}\text{Se}$ (Phase 1) and hexagonal structured $\text{Cu}_{2.001}\text{S}$ (Phase 2); III: orthorhombic structured Cu_2S phase).

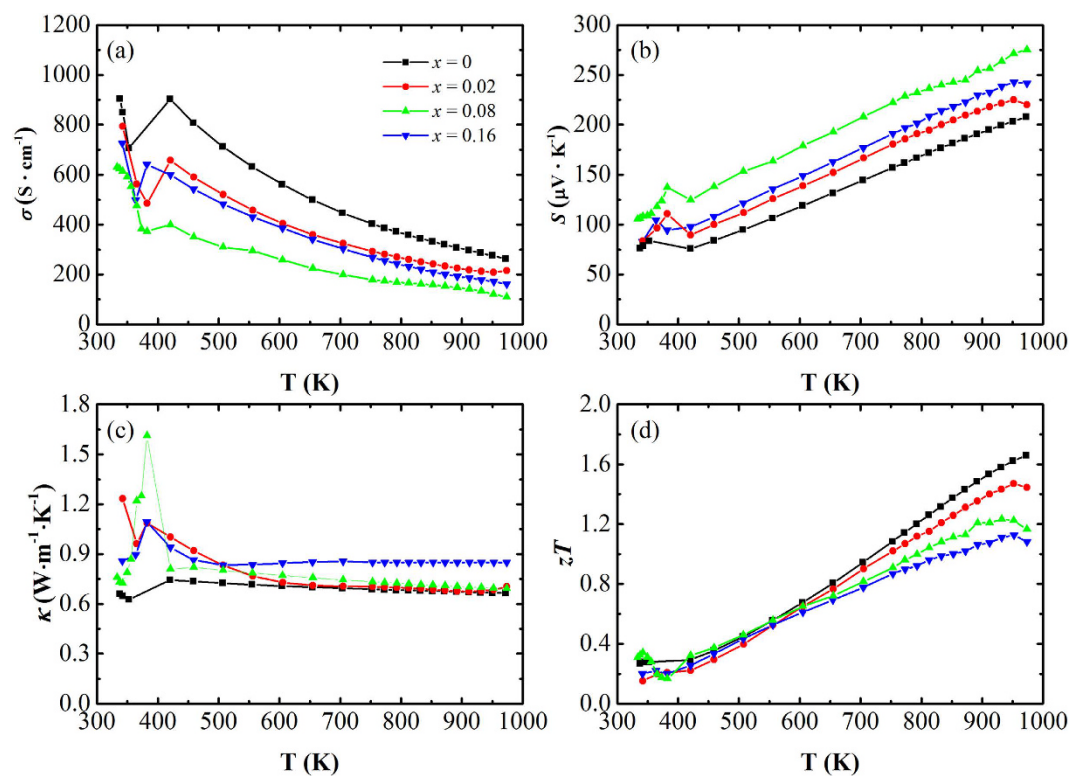


Figure 3. Temperature dependence of thermoelectric properties for the obtained $\text{Cu}_{1.98}\text{S}_x\text{Se}_{1-x}$ ($x = 0, 0.02, 0.08, 0.16$) bulks: (a) electrical conductivity (σ), (b) Seebeck coefficient (S), (c) total thermal conductivity (κ), and (d) dimensionless figure-of-merit (zT).

Figure 3a shows the temperature dependence of the electrical conductivity for the $\text{Cu}_{1.98}\text{S}_x\text{Se}_{1-x}$ ($x = 0, 0.02, 0.08, 0.16$) bulks. It indicates that compared to $\text{Cu}_{1.98}\text{Se}$, the $\text{Cu}_{1.98}\text{S}_x\text{Se}_{1-x}$ ($x = 0.02, 0.08, 0.16$) samples have lower σ values over the whole measured temperature range, and the most obvious difference occurs at $T = 420$ K between $400 \text{ S} \cdot \text{cm}^{-1}$ for the $\text{Cu}_{1.98}\text{S}_{0.08}\text{Se}_{0.92}$ and $900 \text{ S} \cdot \text{cm}^{-1}$ for the $\text{Cu}_{1.98}\text{Se}$. It should be pointed out that this difference becomes less obvious with increasing temperature because the high temperature phases are superionic conductors.

Figure 3b displays the temperature dependence of the Seebeck coefficient for the $\text{Cu}_{1.98}\text{S}_x\text{Se}_{1-x}$ ($x = 0.02, 0.08, 0.16$) bulks. It reveals that the $\text{Cu}_{1.98}\text{S}_x\text{Se}_{1-x}$ ($x = 0.02, 0.08, 0.16$) samples have larger S values than the $\text{Cu}_{1.98}\text{Se}$. Specifically, among all the samples, the $\text{Cu}_{1.98}\text{S}_{0.08}\text{Se}_{0.92}$ has the highest S values, around $275 \mu\text{V} \cdot \text{K}^{-1}$ at $T = 970$ K, which is over 30% higher than that of the $\text{Cu}_{1.98}\text{Se}$.

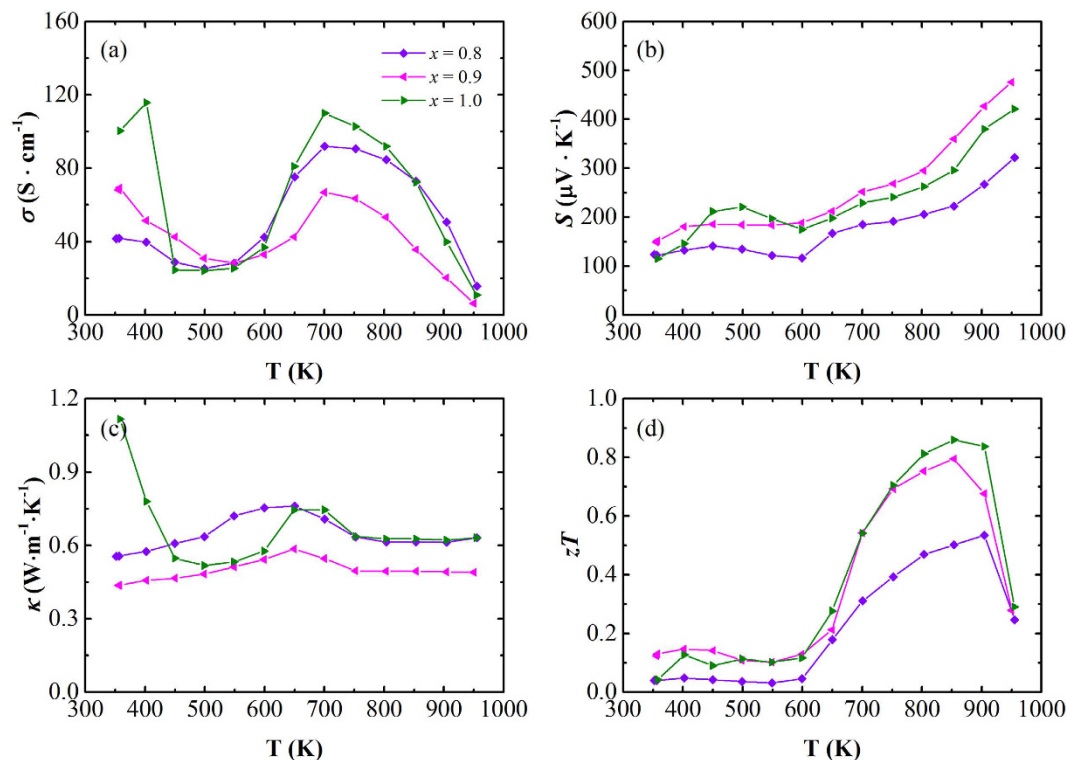


Figure 4. Temperature dependence of the thermoelectric properties for the obtained $\text{Cu}_{1.98}\text{S}_x\text{Se}_{1-x}$ ($x = 0.8, 0.9, 1.0$) bulks: (a) electrical conductivity (σ), (b) Seebeck coefficient (S), (c) total thermal conductivity (κ), and (d) dimensionless figure-of-merit (zT).

Figure 3c shows the temperature dependence of the thermal conductivity for the $\text{Cu}_{1.98}\text{S}_x\text{Se}_{1-x}$ ($x = 0, 0.02, 0.08, 0.16$) bulks. It indicates that both the $\text{Cu}_{1.98}\text{S}_{0.02}\text{Se}_{0.98}$ and $\text{Cu}_{1.98}\text{S}_{0.08}\text{Se}_{0.92}$ bulks have almost the same κ values as the $\text{Cu}_{1.98}\text{Se}$, especially in the temperature range from 500 to 1000 K. The $\text{Cu}_{1.98}\text{S}_{0.16}\text{Se}_{0.84}$, however, shows increased values over the whole temperature range from 300 to 1000 K.

The temperature dependence of the dimensionless figure-of-merit (zT) for the $\text{Cu}_{1.98}\text{S}_x\text{Se}_{1-x}$ ($x = 0, 0.02, 0.08, 0.16$) bulks is shown in Fig. 3d. It should be noted that the $\text{Cu}_{1.98}\text{S}_x\text{Se}_{1-x}$ ($x = 0.02, 0.08, 0.16$) samples show almost the same zT values as the $\text{Cu}_{1.98}\text{Se}$ in the temperature range from 400 to 600 K. Furthermore, they have zT values over 1.0 when $T > 800$ K and exhibit a peak zT at T around 950 K, with the highest value of 1.5 occurring for the $\text{Cu}_{1.98}\text{S}_{0.02}\text{Se}_{0.98}$.

Figure 4 displays the temperature dependence of the electrical conductivity (a), Seebeck coefficient (b), total thermal conductivity (c), and dimensionless figure-of-merit (d) for the obtained $\text{Cu}_{1.98}\text{S}_x\text{Se}_{1-x}$ ($x = 0.8, 0.9, 1.0$) bulks. The results indicate that, for the high temperature cubic structured Cu_2S phase, the $\text{Cu}_{1.98}\text{S}_x\text{Se}_{1-x}$ samples do not show a monotonic increase or decrease in their electrical conductivity compared to the $\text{Cu}_{1.98}\text{S}$. The same trend is also observed for the temperature dependence of the Seebeck coefficient. Furthermore, the $\text{Cu}_{1.98}\text{S}_{0.8}\text{Se}_{0.2}$ sample has almost the same thermal conductivity as the $\text{Cu}_{1.98}\text{S}$, while the $\text{Cu}_{1.98}\text{S}_{0.9}\text{Se}_{0.1}$ sample has much smaller thermal conductivity, with values around $0.5 \text{ W} \cdot \text{m}^{-1} \cdot \text{K}^{-1}$ in the temperature range from 700 to 1000 K. This paradoxical result might be related to the characteristics of the superionic system and the larger radius as well as the heavier mass of selenium compared to sulphur. As aforementioned, the cubic structured Cu_2S is a superionic conductor and it is the migration of copper ions that predominately determines its thermal conductivity. Therefore, the selenium doped samples should have higher thermal conductivity than the $\text{Cu}_{1.98}\text{S}$, due to the enlarged lattice parameters evidenced from the refinements of the X-ray diffraction patterns. On the other hand, selenium is much heavier than sulphur, so the selenium doped samples should have lower thermal conductivity. As a result of these two opposite factors, the samples show the complicated and varying trend that is observed for the thermal conductivity.

The temperature dependence of the dimensionless figure-of-merit shown in Fig. 4d reveals that the selenium doping does not improve the overall thermoelectric performance of the $\text{Cu}_{1.98}\text{S}$ system, with the $\text{Cu}_{1.98}\text{S}$ having the highest zT values around 0.86 at 850 K among all the orthorhombic structured samples, even though certain thermoelectric parameter is enhanced. This observation is in good agreement with our previous reports on the tellurium and iodine doped Cu_{2-x}Se system²¹, which provides further evidence of the distinctiveness of superionic thermoelectric materials in comparison with the conventional thermoelectric materials.

Figure 5 shows a summarized phase diagram for the sulphur doping level dependence of the dimensionless figure-of-merit for the obtained $\text{Cu}_{1.98}\text{S}_x\text{Se}_{1-x}$ ($x = 0, 0.02, 0.08, 0.16, 0.8, 0.9, 1.0$) samples. It indicates that the zT values are first reduced as x increases from 0 to 0.16, and then they are enhanced as x increases from 0.8 to 1.0,

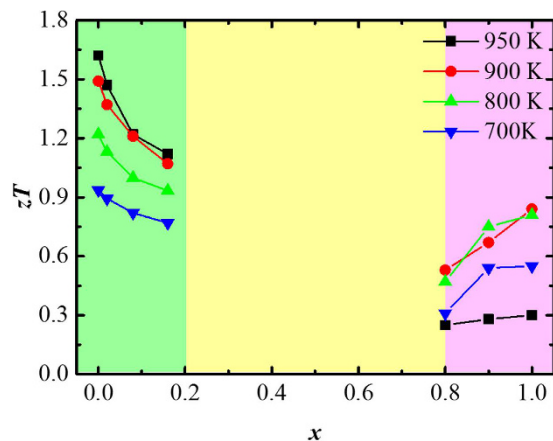


Figure 5. Phase diagram of sulphur doping level dependence of the dimensionless figure-of-merit.

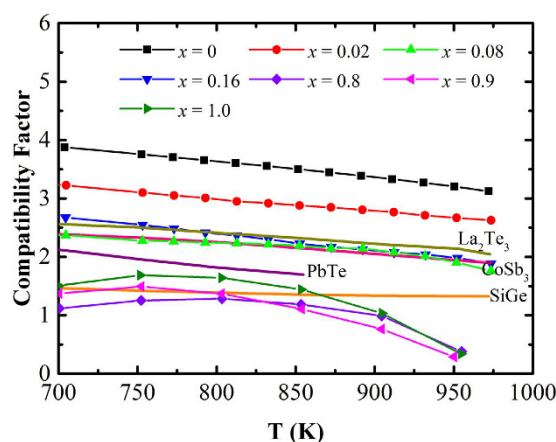


Figure 6. Temperature dependence of the thermoelectric compatibility factor for the $\text{Cu}_{1.98}\text{S}_x\text{Se}_{1-x}$ ($x = 0, 0.02, 0.08, 0.16, 0.8, 0.9, 1.0$) samples.

which agrees very well with our previous theoretical and experimental discussions on sulphur (selenium) doping effects on the superionic $\text{Cu}_{2-x}\text{Se}(\text{S})$ system.

For the practical applications of thermoelectric materials, besides the high zT values that are needed, the thermoelectric compatibility factor, s , is another important factor that needs to be considered when designing an efficient thermoelectric generator^{12,32,35}. The maximum efficiency of a thermoelectric generator will be decreased greatly if the compatibility factors for the segments of n - and p -type thermoelectric materials differ from each other by a factor larger than two. Therefore, in order to discover the best applicable temperature range and best matching material for a certain thermoelectric material, the calculation of s is quite essential.

Figure 6 shows the temperature dependence of the thermoelectric compatibility factor for the $\text{Cu}_{1.98}\text{S}_x\text{Se}_{1-x}$ ($x = 0, 0.02, 0.08, 0.16, 0.8, 0.9, 1.0$) bulks. It indicates that all the samples exhibit stable s values with small fluctuations over a large temperature range from 700 to 1000 K. In the measured temperature range, average s values of around 3.85, 2.92, 2.14, and 2.56 were achieved for the Cu_2Se -phase $\text{Cu}_{1.98}\text{Se}$, $\text{Cu}_{1.98}\text{S}_{0.02}\text{Se}_{0.98}$, $\text{Cu}_{1.98}\text{S}_{0.08}\text{Se}_{0.92}$, and $\text{Cu}_{1.98}\text{S}_{0.16}\text{Se}_{0.84}$ samples, respectively. Furthermore, the Cu_2S -phase samples $\text{Cu}_{1.98}\text{S}_{0.8}\text{Se}_{0.2}$, $\text{Cu}_{1.98}\text{S}_{0.9}\text{Se}_{0.1}$, and $\text{Cu}_{1.98}\text{S}$ exhibit average s values of $\sim 0.72, 0.87$, and 0.93 in the temperature range from 700 to 1000 K, respectively.

For comparison purposes, the s values for some well-known n -type thermoelectric materials are also provided in Fig. 6. It indicates that polycrystalline SiGe, PbTe, La_2Te_3 , and CoSb_3 bulks show s of around 1.37, 1.90, 2.14, and 2.31, respectively. It should be noted that these are very close to the s values of the $\text{Cu}_{1.98}\text{S}_x\text{Se}_{1-x}$ ($x = 0, 0.02, 0.08, 0.16, 0.8, 0.9, 1.0$) bulks, with the differences less than a factor of 2 in the temperature range from 700 to 1000 K. Therefore, a relatively high efficiency could be gained from their coupled thermoelectric modules, which is gratifying for their future practical applications.

As aforementioned in the introduction part, the electrical conductivity and Seebeck coefficient is related to the charge carrier density, carrier mobility, and effective mass, which can be deduced from the calculated DOS and electronic band structures. Therefore, in order to fundamentally understand the strange sulphur doping effects on the thermoelectric properties of the $\text{Cu}_{1.98}\text{S}_x\text{Se}_{1-x}$ system, it is much necessary to do some first-principles calculations on the system's electronic band structures and DOS.

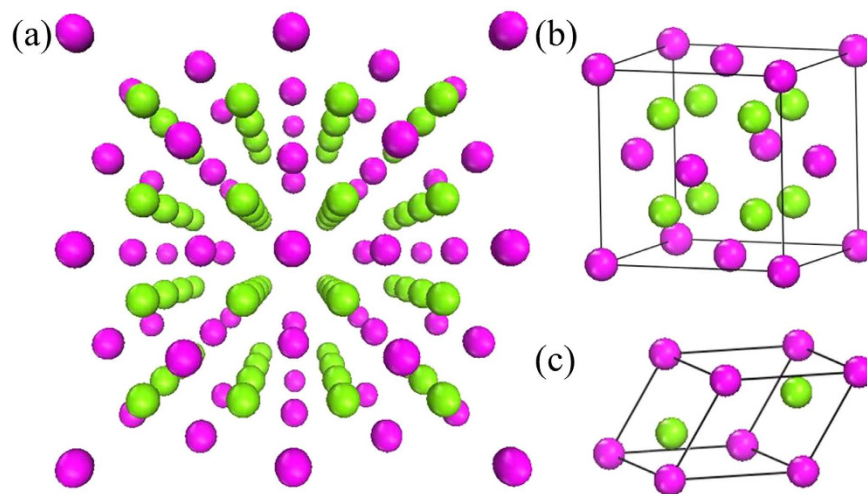


Figure 7. (a) Perspective view of the crystal structure for high temperature cubic structured $\text{Cu}_2\text{Se}(\text{S})$. (b) Ideal version of the unit cell for the cubic structured $\text{Cu}_2\text{Se}(\text{S})$. (c) Primitive cell for the cubic structured $\text{Cu}_2\text{Se}(\text{S})$. Cu and Se(S) atoms are represented by green and purple spheres, respectively.

Figure 7 shows a perspective view of the crystal structures for the cubic structured $\text{Cu}_2\text{Se}(\text{S})$, as well as the ideal versions of the unit cell²² and the primitive cell. It indicates that, in the ideal version of the unit cell for the cubic structured $\text{Cu}_2\text{Se}(\text{S})$ with space group of $Fm\bar{3}m$, the selenium (sulphur) atoms form a face-centred cubic (*fcc*) sub-lattice, and the copper atoms occupy the tetrahedral interstitial positions. It should, however, be noted that $\beta\text{-Cu}_2\text{Se}$ and $\alpha\text{-Cu}_2\text{S}$ have been reported to be superionic conductors, in which the copper ions behave like a liquid^{17,19,36–38}, and they are kinetically disordered throughout the whole structure.

Figure 8 shows the calculated total and partial DOS for the $\text{Cu}_{15}\text{S}_x\text{Se}_{8-x}$ ($x = 1, 2, 4, 6$) compounds. The sulphur doping level dependence of the total and partial DOS at E_F for the $\text{Cu}_{15}\text{S}_x\text{Se}_{8-x}$ ($x = 0, 1, 2, 4, 6, 8$) compounds is displayed in Fig. 9. The results indicate that the DOS at E_F consists of the contributions from the Cu 3d-states, Se 4p-states, and S 3p-states of the $\text{Cu}_{15}\text{S}_x\text{Se}_{8-x}$ compounds, with the Cu 3d-states predominately determining the total DOS at E_F . In addition, the partial DOS for the S atoms obviously increases with increasing x , while the partial DOS for the Se atoms shows the opposite trend, decreasing with increasing x . The total DOS exhibits the same non-monotonic tendency as the partial DOS for the Cu atoms, further indicating that the DOS at E_F for this system is mainly determined by the copper atoms rather than the S or Se atoms. In summary, the total DOS firstly increases slightly, then clearly decreases, with the $\text{Cu}_{15}\text{S}_6\text{Se}_2$ having the highest DOS among all the compounds, ~ 6.29856 states/eV/f.u.

The effective mass can be directly deduced from the calculated DOS based on some references^{13,39}. Figure 10 shows the deduced effective mass for the $\text{Cu}_{15}\text{S}_x\text{Se}_{8-x}$ ($x = 0, 1, 2, 4, 6, 8$) compounds. It indicates that, similar to the DOS, the sulphur doping also has a non-monotonic effect on the effective mass. It firstly has positive effects and gives the $\text{Cu}_{15}\text{S}_4\text{Se}_4$ its highest m^* , with a value of $\sim 1.151 m_e$. It then shows negative effects and results in decreased m^* values as the sulphur doping level increases.

According to Equations 1–4 and previous discussions on σ , S , n and μ , we know that both σ and S are linked to the m^* and the DOS. Specifically, σ is proportional to the carrier density (n) and inversely proportional to m^* . S , however, is proportional to m^* and $\left(\frac{1}{n}\right)^{2/3}$. Therefore, based on the obtained information on the DOS and m^* , we can anticipate the variation trends for the values of S . σ values can also be roughly estimated with disregarding the average scattering time. Hence, we can predict that the cubic structured sulphur doped Cu_{2-x}Se compounds should exhibit non-monotonic variation in σ and S with increasing sulphur concentration according to the calculated DOS and m^* using the DFT method.

It should be pointed out that, for the monoclinic structured Cu_2Se phased $\text{Cu}_{1.98}\text{S}_x\text{Se}_{1-x}$ samples, the observed sulphur doping level dependence of the electrical conductivity and the Seebeck coefficient is in good agreement with the theoretical predictions. The DOS is enhanced as the sulphur doping level increases, while the effective mass is reduced as the doping level increases. Additionally, σ and S are proportional to $\frac{n}{m^*}$ and m^* , respectively. Therefore, enhanced electrical conductivity and reduced Seebeck coefficient can be obtained when the contribution from the DOS is stronger than that from m^* . When the contribution of the effective mass is stronger, decreased electrical conductivity and increased Seebeck coefficient will be achieved.

In summary, the $\text{Cu}_{1.98}\text{S}_x\text{Se}_{1-x}$ compounds have the same crystal structure as monoclinic structured Cu_2Se when $x \leq 0.16$, become composites of cubic structured $\text{Cu}_{1.8}\text{Se}$ and hexagonal structured $\text{Cu}_{2.001}\text{S}$ when $0.2 \leq x \leq 0.7$, and finally have the same crystal structure as orthorhombic structured Cu_2S when $0.8 \leq x \leq 1.0$. The overall thermoelectric performance of the $\text{Cu}_{1.98}\text{S}_x\text{Se}_{1-x}$ compounds is mainly correlated with the electron effective mass and the density of states, with the zT values first increasing and then decreasing. Additionally, all the samples show stable thermoelectric compatibility factors over a broad temperature range from 700 to 1000 K, which could greatly benefit their practical applications. DFT calculations indicate that sulphur doping

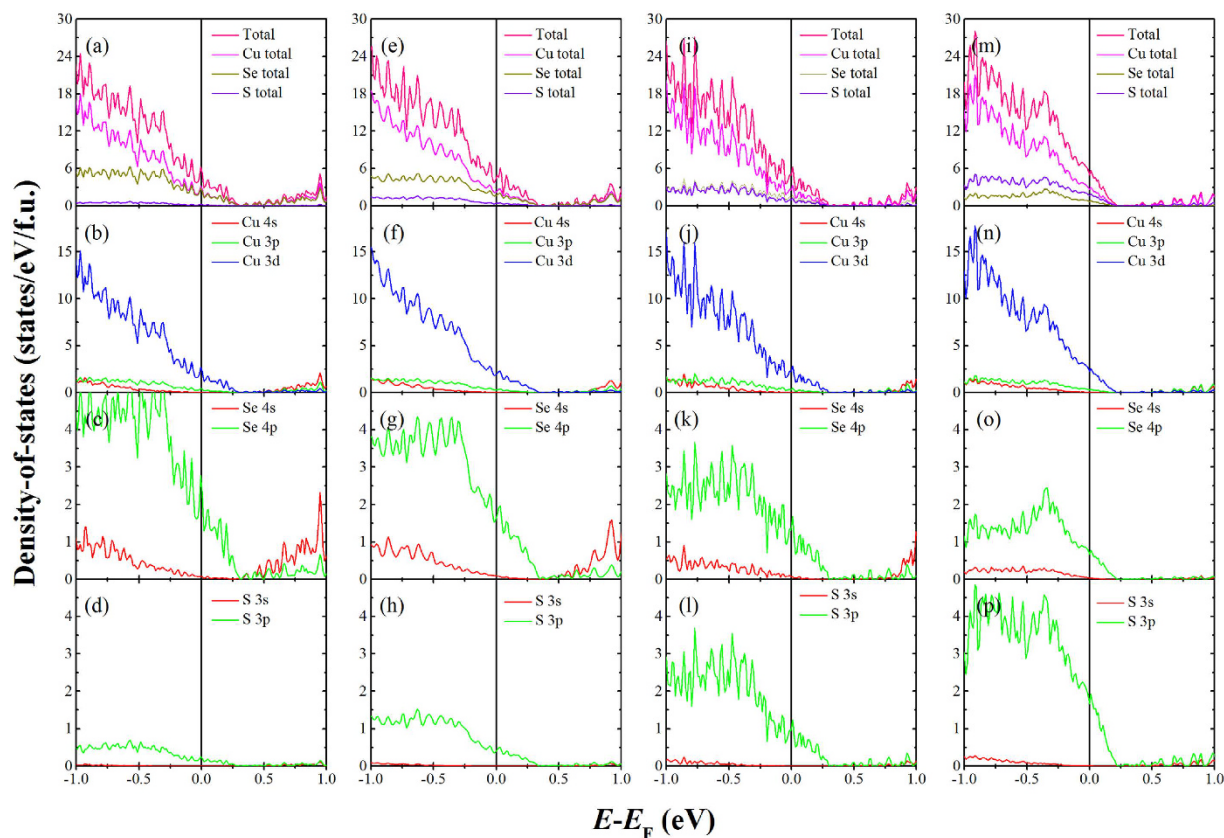


Figure 8. Calculated total and partial density-of-states (DOS) for the $\text{Cu}_{15}\text{S}_x\text{Se}_{8-x}$ ($x = 1, 2, 4, 6$) compounds obtained from the Density Functional Theory calculations. (a,b,c,d) total and partial DOS for the $\text{Cu}_{15}\text{S}_1\text{Se}_7$. (e,f,g,h) total and partial DOS for the $\text{Cu}_{15}\text{S}_2\text{Se}_6$. (i,j,k,l) total and partial DOS for the $\text{Cu}_{15}\text{S}_4\text{Se}_4$. (m,n,o,p) total and partial DOS for the $\text{Cu}_{15}\text{S}_6\text{Se}_2$. The total DOS for the Cu, Se, and S atoms are displayed, and the partial DOS for the 4s-, 3p-, and 3d-states of Cu, the 4s- and 4p-states of Se, and the 3s- and 3p-states of S are also presented. The vertical lines mark the position of the Fermi level (E_F).

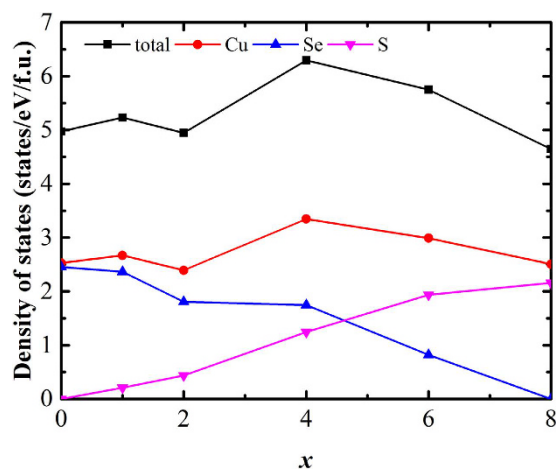


Figure 9. Sulphur doping level dependence of the total and partial density-of-states near the Fermi level for the $\text{Cu}_{15}\text{S}_x\text{Se}_{8-x}$ ($x = 0, 1, 2, 4, 6, 8$) compounds.

has non-monotonic effects on the DOS and m^* , with the $\text{Cu}_{15}\text{S}_6\text{Se}_2$ and $\text{Cu}_{15}\text{S}_4\text{Se}_4$ having the highest DOS value, ~ 0.69 states/eV/f.u., and the highest m^* , $\sim 0.336 m_0$, respectively.

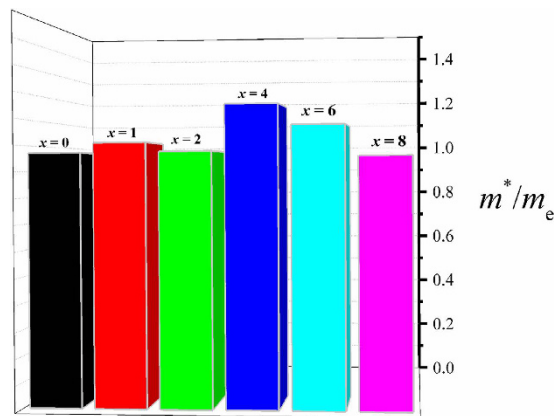


Figure 10. Calculated effective mass for the $\text{Cu}_{15}\text{S}_x\text{Se}_{8-x}$ ($x = 0, 1, 2, 4, 6, 8$) compounds.

Methods

Sample preparation. Polycrystalline $\text{Cu}_{1.98}\text{S}_x\text{Se}_{1-x}$ pellets were synthesized by a conventional solid-state method. Mixtures of Cu, S, and Se powders in the molar ratios of 1.98 : x : 1 - x ($x = 0, 0.02, 0.08, 0.16, 0.2, 0.3, 0.4, 0.5, 0.6, 0.7, 0.8, 0.9, 1.0$) were pressed into pellets and sealed in evacuated quartz tubes, then heated to 873 K for 1–5 hours with a heating rate of 5 K/min, followed by a furnace cooling to room temperature. Finally, the as-sintered pellets were used in a melt-solidification approach to achieve highly dense polycrystalline bulks, which has been described in detail in our previous work^{19,21}. The obtained polycrystalline bulks were then shaped into round disks and rectangular bulks for electrical conductivity and thermal diffusivity measurements, respectively.

Measurements. X-ray diffraction (XRD) patterns were collected on a GBC MMA system using Cu K α radiation. The electrical conductivity and Seebeck coefficient were measured simultaneously in a helium atmosphere from 300 to 973 K using an RZ2001i system. The thermal diffusivity (D) was measured by the laser flash method (LINSEIS LFA 1000), and the specific heat (C_p) was determined by differential scanning calorimetry (NETZSCH DSC 204F1). The sample density (dd) was determined by the sample mass divided by volume, and the thermal conductivity (κ) was calculated according to $\kappa = D \times C_p \times dd$.

Calculations. The calculations of electronic band structures, and total and partial DOS were performed based on the DFT method, implemented by the CASTEP package⁴⁰ with the generalized gradient approximation (GGA)⁴¹. The calculations were parameterized by the Perdew-Burke-Ernzerhof (PBE)⁴² and ultra-soft pseudo-potentials. The plane wave cut-off energy was set at 400 eV. For Cu_2Se and Cu_2S , a primitive cell with the Brillouin zone path of $\Gamma\text{XW}\Gamma\text{K}$ (Fig. S1 in Electronic Supplementary Information) was employed for the band structure calculations. For the $\text{Cu}_{15}\text{S}_x\text{Se}_{8-x}$ ($x = 0, 1, 2, 4, 6, 8$), geometry optimizations were performed on a $2 \times 2 \times 2$ supercell, with one copper atom deleted, of the Cu_2Se primitive cell. Then, the Brillouin zone path of $\Gamma\text{XW}\Gamma\text{K}$ and a k-point set of $15 \times 15 \times 15$ for the supercell were used to calculate the electronic band structures, and the total and partial DOS, respectively.

References

- Zeier, W. G. *et al.* Phonon scattering through a local anisotropic structural disorder in the thermoelectric solid solution $\text{Cu}_2\text{Zn}_{1-x}\text{Fe}_x\text{GeSe}_4$. *J. Am. Chem. Soc.* **135**, 726–732, doi: 10.1021/ja308627v (2013).
- Liu, W., Yan, X., Chen, G. & Ren, Z. Recent advances in thermoelectric nanocomposites. *Nano Energy* **1**, 42–56, doi: 10.1016/j.nanoen.2011.10.001 (2012).
- Jood, P. *et al.* Al-doped zinc oxide nanocomposites with enhanced thermoelectric properties. *Nano Lett.* **11**, 4337–4342, doi: 10.1021/nl202439h (2011).
- Zhang, Y., Wang, X. L., Yeoh, W. K., Zheng, R. K. & Zhang, C. Electrical and thermoelectric properties of single-wall carbon nanotube doped Bi_2Te_3 . *Appl. Phys. Lett.* **101**, 031909, doi: 10.1063/1.4737898 (2012).
- Pei, Y. *et al.* Convergence of electronic bands for high performance bulk thermoelectrics. *Nature* **473**, 66–69, doi: 10.1038/nature09996 (2011).
- Pei, Y. *et al.* Optimum Carrier Concentration in n-Type PbTe Thermoelectrics. *Adv. Energy Mater.* **4**, 1400486, doi: 10.1002/aenm.201400486 (2014).
- Yamini, S. A. *et al.* Chemical composition tuning in quaternary p-type Pb-chalcogenides—a promising strategy for enhanced thermoelectric performance. *Phys. Chem. Chem. Phys.* **16**, 1835–1840, doi: 10.1039/c3cp54493a (2014).
- Pei, Y., Heinz, N. A. & Snyder, G. J. Alloying to increase the band gap for improving thermoelectric properties of Ag_2Te . *J. Mater. Chem.* **21**, 18256, doi: 10.1039/c1jm13888j (2011).
- Wang, H., Pei, Y., LaLonde, A. D. & Snyder, G. J. Heavily doped p-type PbSe with high thermoelectric performance: an alternative for PbTe. *Adv. Mater.* **23**, 1366–13370, doi: 10.1002/adma.201004200 (2011).
- Cutler, M., Leavy, J. & Fitzpatrick, R. Electronic Transport in Semimetallic Cerium Sulfide. *Phys. Rev.* **133**, A1143–A1152, doi: 10.1103/PhysRev.133.A1143 (1964).
- Bulusu, A. & Walker, D. G. Review of electronic transport models for thermoelectric materials. *Superlattice Microst.* **44**, 1–36, doi: 10.1016/j.spmi.2008.02.008 (2008).
- Snyder, G. J. & Toberer, E. S. Complex thermoelectric materials. *Nat. Mater.* **7**, 10 (2008).
- Lange, B., Freysoldt, C. & Neugebauer, J. Native and hydrogen-containing point defects in Mg_3N_2 : A density functional theory study. *Phys. Rev. B* **81**, 224109, doi: 10.1103/PhysRevB.81.224109 (2010).

14. Parker, D., Chen, X. & Singh, D. J. High three dimensional thermoelectric performance from low dimensional bands. *Phys. Rev. Lett.* **110**, 146601 (2013).
15. Sun, B. Z., Ma, Z., He, C. & Kechen, W. Anisotropic thermoelectric properties of layered compounds in SnX₂ (X = S, Se): A promising thermoelectric material. *Phys. Chem. Chem. Phys.*, doi: 10.1039/c5cp03700j (2015).
16. Dennler, G. *et al.* Are Binary Copper Sulfides/Selenides Really New and Promising Thermoelectric Materials? *Adv. Energy Mater.* **4**, 1301581, doi: 10.1002/aenm.201301581 (2014).
17. Liu, H. *et al.* Copper ion liquid-like thermoelectrics. *Nat. Mater.* **11**, 422–425, doi: 10.1038/nmat3273 (2012).
18. He, Y. *et al.* High thermoelectric performance in non-toxic earth-abundant copper sulfide. *Adv. Mater.* **26**, 3974–3978, doi: 10.1002/adma.201400515 (2014).
19. Zhao, L. *et al.* Superior intrinsic thermoelectric performance with zT of 1.8 in single-crystal and melt-quenched highly dense Cu_{2-x}Se bulks. *Sci. Rep.* **5**, 7671, doi: 10.1038/srep07671 (2015).
20. Zhao, L. *et al.* High thermoelectric and mechanical performance in highly dense Cu_{2-x}S bulks prepared by a melt-solidification technique. *J. Mater. Chem. A* **3**, 9432–9437, doi: 10.1039/c5ta01667c (2015).
21. Zhao, L. *et al.* The Effects of Te²⁻ and I⁻ Substitutions on the Electronic Structures, Thermoelectric Performance, and Hardness in Melt-Quenched Highly Dense Cu_{2-x}Se. *Advanced Electronic Materials* **1**, 1400015, doi: 10.1002/aeml.201400015 (2015).
22. Rasander, M., Bergqvist, L. & Delin, A. Density functional theory study of the electronic structure of fluorite Cu₂Se. *J. Phys. Condens. Matter.* **25**, 125503, doi: 10.1088/0953-8984/25/12/125503 (2013).
23. Ballikaya, S., Chi, H., Salvador, J. R. & Uher, C. Thermoelectric properties of Ag-doped Cu₂Se and Cu₂Te. *J. Mater. Chem. A* **1**, 12478, doi: 10.1039/c3ta12508d (2013).
24. Ibáñez, M. *et al.* Colloidal synthesis and thermoelectric properties of Cu₂SnSe₃ nanocrystals. *Journal of Materials Chemistry A* **1**, 1421, doi: 10.1039/c2ta00419d (2013).
25. Suzumura, A., Watanabe, M., Nagasako, N. & Asahi, R. Improvement in Thermoelectric Properties of Se-Free Cu₃SbS₄ Compound. *J Electron Mater* **43**, 2356–2361, doi: 10.1007/s11664-014-3064-y (2014).
26. Zhong, B. *et al.* High superionic conduction arising from aligned large lamellae and large figure of merit in bulk Cu_{1.94}Al_{0.02}Se. *Appl. Phys. Lett.* **105**, 123902, doi: 10.1063/1.4896520 (2014).
27. Fan, J. *et al.* Crystal Structure and Physical Properties of Ternary Phases around the Composition Cu₅Sn₂Se₇ with Tetrahedral Coordination of Atoms. *Chem Mater* **26**, 5244–5251, doi: 10.1021/cm501899q (2014).
28. Tyagi, K. *et al.* Thermoelectric and mechanical properties of spark plasma sintered Cu₃SbSe₃ and Cu₃SbSe₄: Promising thermoelectric materials. *Appl. Phys. Lett.* **105**, 261902, doi: 10.1063/1.4904996 (2014).
29. Liu, H. *et al.* Ultrahigh thermoelectric performance by electron and phonon critical scattering in Cu₂Se_{1-x}I_x. *Adv. Mater.* **25**, 6607–6612, doi: 10.1002/adma.201302660 (2013).
30. Snyder, G. J. Application of the compatibility factor to the design of segmented and cascaded thermoelectric generators. *Appl. Phys. Lett.* **84**, 2436, doi: 10.1063/1.1689396 (2004).
31. Snyder, G. & Ursell, T. Thermoelectric efficiency and compatibility. *Phys. Rev. Lett.* **91**, 148301, doi: 10.1103/PhysRevLett.91.148301 (2003).
32. Snyder, G. J. & Caillat, T. Using the compatibility factor to design high efficiency segmented thermoelectric generators. *MRS Proceedings* **793**, 37–42 (2003).
33. Bhardwaj, A., Chauhan, N. S. & Misra, D. K. Significantly enhanced thermoelectric figure of merit of p-type Mg₃Sb₂-based Zintl phase compound via nanostructuring employing high energy mechanical milling coupled with spark plasma sintering. *J. Mater. Chem. A* **3**, 10777, doi: 10.1039/c5ta02155c (2015).
34. Gulay, L., Daszkiewicz, M., Strok, O. & Pietraszko, A. Crystal structure of Cu₂Se. *Chem. Met. Alloys* **4**, 200–205 (2011).
35. Ursell, T. S. & Snyder, G. J. Compatibility of Segmented Thermoelectric Generators. *Twenty-First International Conference on Thermoelectrics*, 412–417 (2002).
36. Oliveria, M., McMullan, R. K. & Wuensch, B. J. Single crystal neutron diffraction analysis of the cation distribution in the high-temperature phases a-Cu₂-xS, a-Cu₂-xSe, AND a-Ag₂Se. *Solid State Ion.* **28-30**, 1332–1337 (1988).
37. Heyding, R. D. & Murry, R. M. The crystal structures of Cu_{1.8}Se, Cu₃Se₂, α- and γ-CuSe, CuSe₂ and CuSe₂ II. *Can. J. Chem.* **54**, 841–848 (1976).
38. Lu, P. *et al.* Multiformality and fluctuation of Cu ordering in Cu₂Se thermoelectric materials. *J. mater. Chem. A* **3**, 6901–6908, doi: 10.1039/C4TA07100J (2015).
39. Jaworski, C. M., Wiendlocha, B., Jovicic, V. & Heremans, J. P. Combining alloy scattering of phonons and resonant electronic levels to reach a high thermoelectric figure of merit in PbTeSe and PbTeS alloys. *Energy Environ. Sci.* **4**, 4155, doi: 10.1039/c1ee01895g (2011).
40. Clark, S. J. *et al.* First principles methods using CASTEP. *Z. Kristallogr.* **220**, 567–570 (2005).
41. Hohenberg, P. Inhomogeneous electron gas. *Phys. Rev.* **136**, B864–B871, doi: 10.1103/PhysRev.136.B864 (1964).
42. Perdew, J. P., Burke, K. & Ernzerhof, M. Generalized Gradient Approximation Made Simple. *Phys. Rev. Lett.* **77**, 3865–3868 (1996).

Acknowledgements

X.L.W. acknowledges the support for this work from the Australian Research Council (ARC) through an ARC Discovery Project (DP 130102956) and an ARC Professorial Future Fellowship project (FT 130100778) and an ARC LIEF project (LE120100069, X.L.W.). L.L.Z. is grateful for the support from the Fundamental Research Funds of Shandong University (11160076614087) and the Natural Science Foundation of Shandong Province (ZR2013EMM014 and ZR2013EMM018). J.W. is grateful for the support from the Fundamental Research Funds of Shandong University (31370076614103). The authors would like to thank Prof. G. Jeffrey Snyder (Northwestern University) for helpful discussions on the calculations and experimental results. The authors would also thank Dr. Tania Silver for polishing the English of the manuscript.

Author Contributions

X.L.W. and L.L.Z. designed the experiments and theoretical calculations. L.L.Z. and J.W. fabricated samples and performed the XRD and measurements. L.L.Z., F.Y.F., F.N.W., C.L.W. and J.C.L. did the theoretical calculations. L.L.Z., F.Y.F., J.W., F.N.W., C.L.W., J.C.L., J.Y.W., Z.X.C., S.X.D., and X.L.W. analyzed and discussed the data. All authors reviewed the manuscript.

Additional Information

Supplementary information accompanies this paper at <http://www.nature.com/srep>

Competing financial interests: The authors declare no competing financial interests.

How to cite this article: Zhao, L. *et al.* Improvement of thermoelectric properties and their correlations with electron effective mass in $\text{Cu}_{1.98}\text{S}_x\text{Se}_{1-x}$. *Sci. Rep.* 7, 40436; doi: 10.1038/srep40436 (2017).

Publisher's note: Springer Nature remains neutral with regard to jurisdictional claims in published maps and institutional affiliations.



This work is licensed under a Creative Commons Attribution 4.0 International License. The images or other third party material in this article are included in the article's Creative Commons license, unless indicated otherwise in the credit line; if the material is not included under the Creative Commons license, users will need to obtain permission from the license holder to reproduce the material. To view a copy of this license, visit <http://creativecommons.org/licenses/by/4.0/>

© The Author(s) 2017